Meteoritics & Planetary Science 38, Nr 9, 1319–1330 (2003)
Abstract available online at http://meteoritics.org

Ice dynamics of the Allan Hills meteorite concentration sites revealed by satellite aperture radar interferometry

F. COREN,[1] G. DELISLE,[2*] P. STERZAI[1]

[1]National Institute of Oceanography and Applied Geophysics (OGS), Borgo Grotta Gigante 42/c, I-34010–Sgonico, Trieste, Italy
[2]Bundesanstalt für Geowissenschaften und Rohstoffe (BGR), Stilleweg 2, D-30655 Hannover, Germany

[*]Corresponding author. E-mail: G.Delisle@bgr.de

(Received 05 August 2002; revision accepted 03 September 2003)

Abstract–The ice flow conditions of a 100 × 100 km area of Victoria Land, Antarctica were analyzed with the synthetic aperture radar (SAR) technique. The area includes a number of meteorite concentration sites, in particular the Allan Hills ice fields. Regional ice flow velocities around the Mid-western and Near-western ice fields and the Allan Hills main ice field are shown to be ≤2.5 m yr^{-1}. These sites are located on a horseshoe-shaped area that bounds an area characterized by higher ice flow velocities of up to 5 m yr^{-1}. Meteorite find locations on the Elephant Moraine are located in this "high ice flow" area. The SAR derived digital elevation model (DEM) shows atypical low surface slopes for Antarctic conditions, which are the cause for the slow ice movements. Numerous ice rises in the area are interpreted to cap sub-ice obstacles, which were formed by tectonic processes in the past. The ice rises are considered to represent temporary features, which develop only during warm stages when the regional ice stand is lowered. Ice depressions, which develop in warm stages on the lee side of ice rises, may act as the sites of temporary build-up of meteorite concentrations, which turn inoperative during cold stages when the regional ice level rises and the ice rises disappear. Based on a simplified ice flow model, we argue that the regional ice flow in cold stages is reduced by a factor of at least 3.

INTRODUCTION

A large number of meteorites have been collected since 1976 on the blue ice fields west of the Allan Hills in Victoria Land, Antarctica. Five key sites with major meteorite concentrations are known. They are the main Allan Hills Icefield (AHI), about 5 km to the west of the Allan Hills, the Near-western, Mid-western and Far-western Icefields (NWI, MWI, and FWI) to the west and south-west, and an extended series of blue ice fields between the Elephant Moraine (EM) and Reckling Peak to the northwest of the Allan Hills (Fig. 1). The ice flow dynamics causing the high meteorite concentrations were repeatedly the subject of investigations. The barrier-concept outlined in Cassidy and Rancitelli (1982) and Whillans and Cassidy (1983) has proven correct in the sense that all later studies concluded that barriers, exposed or hidden under a thin layer of ice, cause a significant slow-down of ice flow so that the amount of advected ice to the area in question is of the same order or less than the amount of ice sublimated into the atmosphere. Meteorites enclosed in ice travel to the meteorite concentration site, where, while the enclosing ice is sublimated, meteorites are left behind on the ice surface. The ice flow in the immediate vicinity of the AHI is much better known in comparison to the ice fields of the more distant meteorite concentration sites. This paper attempts to close this gap of knowledge by taking advantage of the synthetic aperture radar interferometry (INSAR) technique. Based on satellite imagery acquired by ERS-1 and ERS-2 satellites and provided by the VECTRA (ESA-A.O. 3–108) project, we present new data on surface topography, surface ice slope, ice velocities, and to some extent, ice thickness. With this new compilation, we develop an expanded picture of the current and past ice flow conditions that have prevailed in the area and caused the build-up of the meteorite concentration sites of today.

Previous Work

The first meteorite finds near the Allan Hills were made in the 1976/77 field season (Cassidy et al. 1977). Early methods used to survey the area centered around a triangulation survey (Nishio and Annexstad 1979; Annexstad

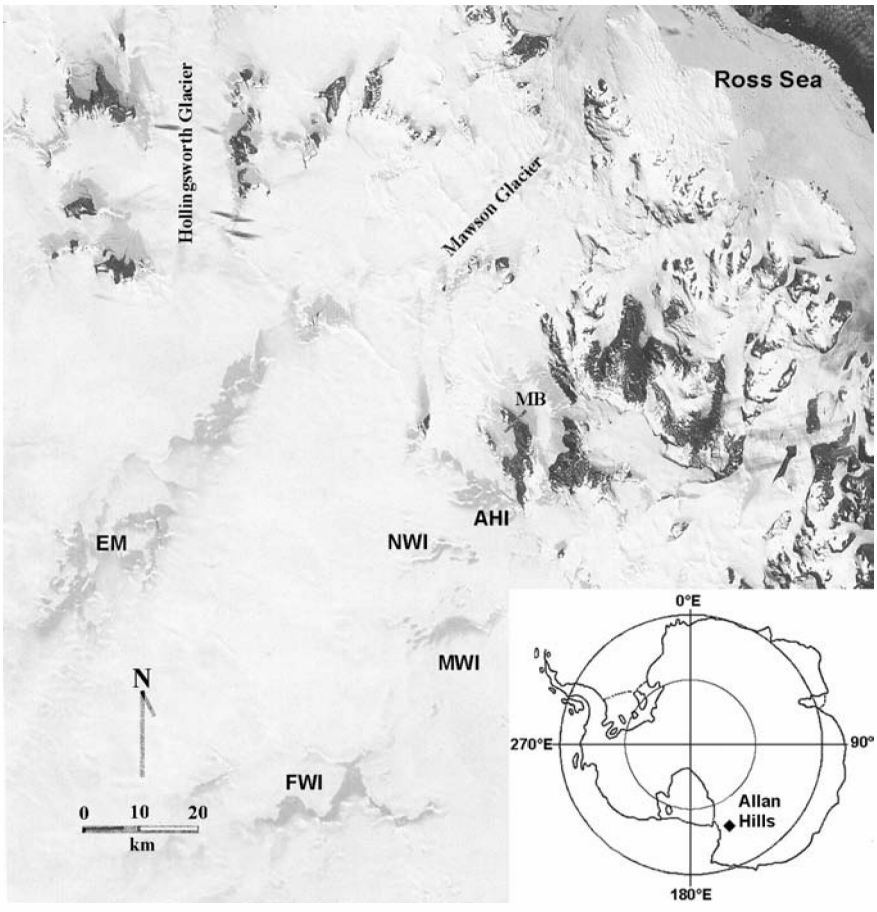

Fig. 1. Satellite image of Victoria Land. Blue ice fields with high meteorite concentrations are shown; AHI: Allan Hills Icefield; NWI: Near-western Icefield; MWI: Mid-western Icefield; FWI: Far-western Icefield. MB denotes Manhaul Bay to the east of the Allan Hills. The Ross Sea is visible in the upper right corner of image (from Cassidy et al. 1992).

and Nishio 1980; Annexstad and Schultz 1982; Schultz et al. 1990), a gravity survey (Fudali 1982) to investigate and to calculate ice thickness and bedrock topography, and mathematical modeling of ice flow by van Heeswijk (1984). Varying ice stands of the regional ice fields in response to climate change were elaborated upon by Cassidy (1983) and Zolensky (1998). They considered it likely that higher ice stands during climatically cold stages caused the removal of meteorite accumulations by ice flow across former ice flow barriers. A numerical model on the response of the Antarctic ice sheet to global change by Delisle (1993) suggested that the concentration of all meteorite concentration sites along the 2000 m elevation line might be caused by the existence of a hinge line on the Antarctic ice sheet at an elevation of about 2000 m, which, during cold stages, separates the growing ice stand in coastal regions from the shrinking ice stand in the Antarctic interior (and vice versa in warm stages). The re-survey of the triangulation net in the 1988/89 field season resulted in well-restrained data on ice flow velocities across the AHI. A ground based radar survey in the same season revealed a complex sub-ice topography below the AHI and NWI (Delisle and Sievers 1991), which, back in the early Cenozoic, had been shaped before and during the onset of Antarctic glaciation (Delisle 1997). The ground-based radar and triangulation surveys showed the AHI and NWI to be separated by a northward flowing ice stream suggesting slightly different ice source areas and slightly separate meteorite concentration histories, which might actually be reflected by different natural thermoluminescence data on meteorites from both sites (Benoit et al. 1993). The ^{26}Al, ^{10}Be, 2.8 Ma age of ablation debris from the passage of a large H-group ordinary chondrite found in a dust layer of AHI suggests a longtime stability of the regional ice flow conditions (Harvey et al. 1998). An extensive summary of our knowledge of meteorite concentration sites in Antarctica can be found in Cassidy et al. (1992).

The Synthetic Aperture Radar Interferometry Method

The INSAR method is capable of producing, from a series of radar images, an elevation model (topography) and a map of displacement rates (ice flow velocity) of an area, if

certain favorable conditions that usually prevail in high latitude glaciatied terrain are met. The principles of this technique are described, e.g., in König et al. (2001), Gabriel et al. (1989), and Goldstein et al. (1993). We have investigated an approximately 100 × 100 km area around the AHI, bounded by the following coordinates:

Western corner: 76°15′ S, 156°45′ E
Northern corner: 75°45′ S, 160°00′ E
Eastern corner: 76°45′ S, 161°30′ E
Southern corner: 77°00′ S, 158°00′ E

SAR scenes acquired by the ERS-1 and ERS-2 satellites and provided by the VECTRA (ESA-A.O. 3-108) project were used to compute a digital elevation model (DEM) for this area and the ice flow velocity field in satellite sight direction by interferometry. The SAR images were mutually co-registered to a sub-pixel accuracy level, adopting interative processes. Interferograms and coherence images were formed. We found that both image pairs and acquisitions made 70 days apart achieved high coherence across the whole scene and, hence, yielded high quality fringes, enabling us to process the entire frame fully (Fig. 2). Flat earth frequency has been removed using the ellipsoidal earth WGS-84; the same reference was also adopted to derive the maps shown in Figs. 2–4 and Fig. 6. Baselines were initially estimated using Delft Precise Orbit data (Scharroo and Visser 1998). The topographic phase was isolated by differentiating image$_{1,2}$ ($I_{1,2}$; Fig. 3) from $I_{3,4}$ (Rignot et al. 1996a, b) under the assumption that the velocity field remains constant between the 2 acquisitions over the relevant 70 day period (see Table 1). The combination of the normal baseline (Bn $I_{1,2}$ >Bn $I_{3,4}$) assumes that the first tandem is much more sensitive to topography than the second one and that the resultant topographic interferogram (Fig. 3) also represents a favorable baseline (121 m corresponding to 74 m of altitude ambiguity). Elevation ambiguity has been solved by phase-unwrapping, and we corrected the resultant interferometric DEM using ground control points (GCP) derived from an existing low-resolution digital model by Bamber and Bindschadler (1998) and a few published elevation data (Cassidy et al. 1983) from the area. We use a

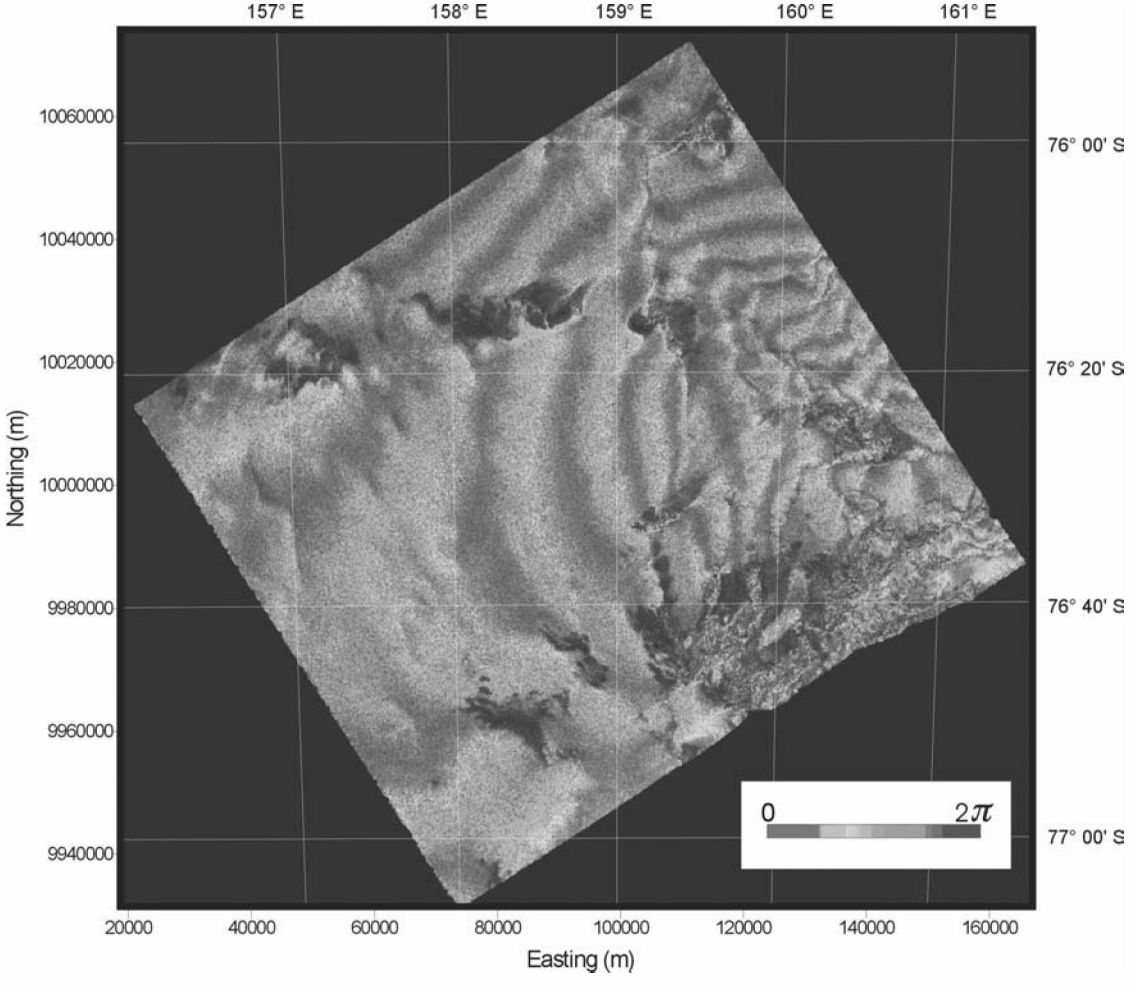

Fig. 2. Geocoded interferogram (topographic component) derived by differentiation of 2 tandem acquisition interferograms 70 days apart. The resultant baseline is 121 m. Every phase cycle corresponds approximately to an elevation of 74 m.

Table 1. List of SAR scenes used in this study.

Ref. orbit	Image num.	Ref. date	Interf. orbit	Image num.	Interf. date	Elapsed time	B_{perp} (m)[a]	Ambig. height (m)[b]
E1–23949	1	1996.02.12	E2–04276	2	1996.02.13	1 day	~132	~68
E1–24951	3	1996.04.22	E2–05278	4	1996.04.23	1 day	~13	~692

[a]Perpendicular component of baseline at mid-swath.
[b]Ambiguity height at mid-swath.

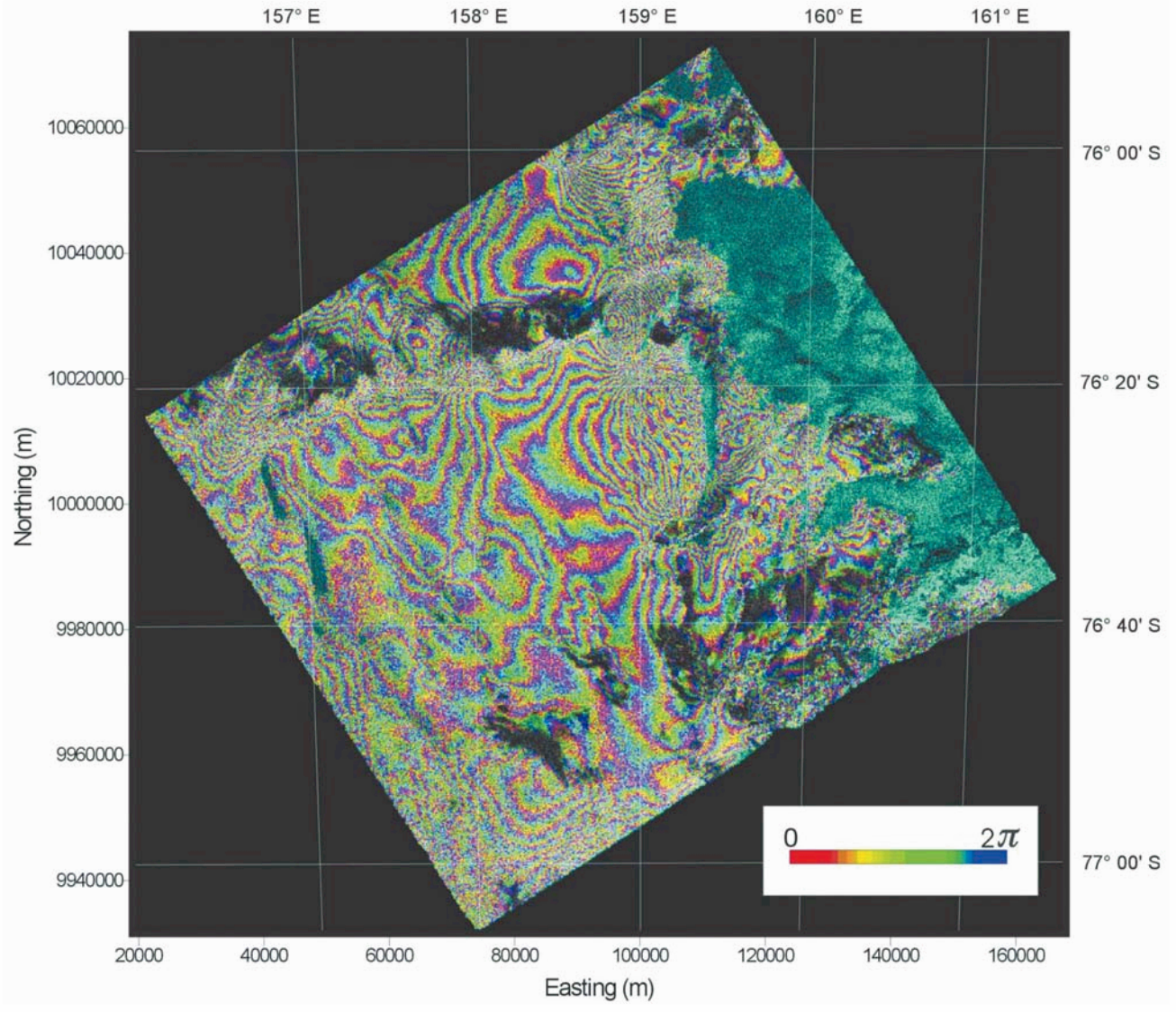

Fig. 3. Geocoded interferogram (motion component) with 70 days temporal baseline after removal of the topographic component (see Fig. 2). Every phase cycle corresponds to 28.8 mm displacement in the satellite line-of-sight direction.

total of 21 ground control points (GCP), achieving a root mean squared (rms) error between the GCP and the correspondent SAR-DEM elevation of 9.8 m. We cannot evaluate effectively the accuracy of the presented DEM because of the lack of other independent reference GCP, even though we presume that a maximum root mean squared error of 50 m can be assumed. The DEM (Fig. 4; see also Fig. 7) shows a series of subparallel snow or ice ridges, which are interpreted to delineate the main tectonic features under an almost flat and slightly inclined to the north snow/ice surface. The drop in elevation to the south of the MWI might be an artifact due to induced errors. A further refinement of the DEM could be reached by additional differential Global Positioning System (GPS) measurements in the area to better constrain the

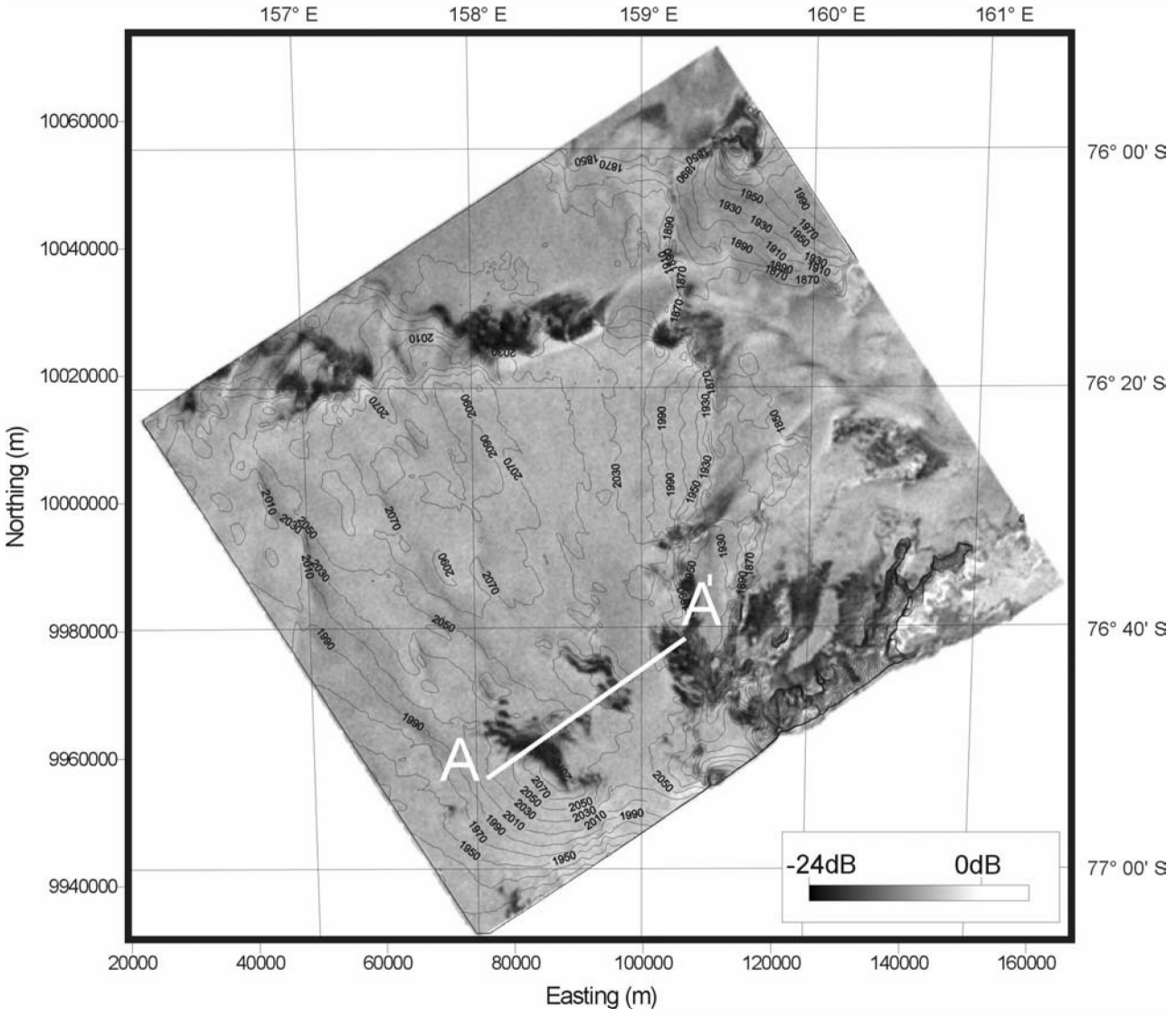

Fig. 4. Digital elevation model with elevation contour lines superimposed on the SAR amplitude image.

baseline. One single SAR image has been geocoded using the INSAR DEM. This image furnishes the base map of Fig. 4, where DEM contour lines are superimposed.

Areas of blue ice, characterized by low backscattering values, are easy to spot. They show up in dark colors on the DEM. The plot (Fig. 5) of the backscattering coefficient $\sigma 0$ along profile A-A′ in Fig. 4 shows the interrelation between the occurrence of blue ice fields (indicated as dark bands on the bottom of Fig. 5) and the reduction of the backscattering effect.

The ice surface velocity field in the area spans between 0 and 0.010 m/day, which is related in satellite line-of-sight to a maximum of 0.004 m or 0.13 fringes/day. This magnitude of displacement cannot be recovered easily using tandem images (one day temporal baseline). Therefore, we combined ERS-1 acquisitions of images 70 days apart, as $I_{1,3}$ (Table 1), to increase the displacement component in the interferogram with respect to the topographic one. We use the interferometric DEM to simulate an interferogram with the same baseline of $I_{1,3}$ (139 m baseline), and then, we differentiated them to recover an interferogram, which records the motion component only (Fig. 6). After the phase-unwrapping procedure, we computed the displacement in satellite line-of-sight (LOS) and then derived the horizontal components that occurred between the acquisitions that were 70 days apart. The derived ice flow velocity field was then converted to m yr^{-1} values. The amplitude images were also used to characterize the different types of ice within the area.

Synthesis of SAR Data With Ground Observations

The information obtained by the SAR method is ambiguous in several ways. The DEM identifies, with an accuracy previously unobtained, surface features of the investigated area but, however, does not identify the exact

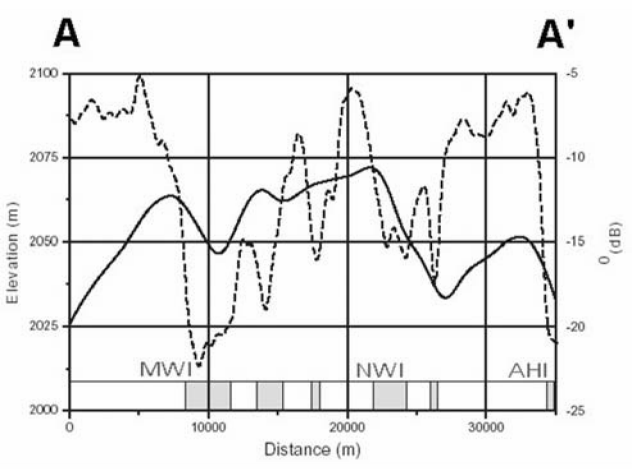

Fig. 5. Plot of the backscattering coefficient σ0 (striped line) and elevation (black line) along the profile marked as A-A′ in Fig. 4. The lower bar indicates the type of ice present along the profile. The gray blocks indicate the presence of blue ice. Blue ice fields are located along the northeastern side of ice ridges (the lee side of prevailing wind direction).

altitude of these features because of insufficient number of ground reference points (see above). The SAR-derived velocity field is based on a statistical analysis of the magnitude of displacements on a pixel by pixel basis. However, it does not, per se, produce a map with the exact direction of the ice movements. Latter information must be inferred from surface observations on ice flow directions and ice slope. With these limitations in mind, we can, nevertheless, derive new details on the tectonic and glaciological situation in the area.

The Surface Topography and Ice Surface Slope Images

The DEM (Fig. 4) indicates several features. The set of northwest-southeast running ridges west of the Allan Hills, the pronounced southwest-northeast escarpment along the EM (L1 in Fig. 7), and the south to north oriented lineament running from the southern tip of the Allan Hills via Battlement Nunatak and Reckling Peak (L2 in Fig. 7) are the most prominent of these features. To enhance the topographic expression of these features, we present a shaded relief representation of the DEM (Fig. 7). The L1 lineament extends at least from the EM via Reckling Peak to the coast. The second lineament (L2) is interrupted by L1 and continues north of L1 toward the Hollingsworth Glacier.

The Ice Flow Velocity Image

Fig. 6 shows the distribution of ice flow velocities in the investigated area, as far as the applied methodology for SAR-interferometry interpretation was able to resolve flow components. The derived ice flow directions show the following main features:

- A zone extending from EM via MWI to the AHI encloses an area of ice that flows with velocities between 2.5 to 5 m yr^{-1}. Based on the position of the derived elevation lines (Fig. 4) and in agreement with earlier investigations and field observations (Faure and Taylor 1985), this ice passes the Elephant Moraine on its eastern flank and continues northward to the catchment area of the David Glacier.
- Ice flow appears to decelerate from the center of the MWI in all directions.
- The ice flow velocities around the NWI are very low. The 1.5 m yr^{-1} contour line almost encloses the NWI rise and suggests radial flow away from the rise.
- The area between the NWI and AHI is characterized by ice flow with ice flow velocities of on average 1 m yr^{-1}, which is in excellent agreement with data previously reported by Schultz et al. (1990). Part of this ice flow appears to turn to the northwest, implying eventual drainage into the David Glacier, and part of it spills over sub-ice obstructions toward the catchment area of the Mawson Glacier.
- The ice flow velocities along the western foot of the Allan Hills and along the western slope of the AHI are in agreement with results of previous measurements (Schultz et al. 1990).

DISCUSSION

These results allow us to gain new insight concerning the regional tectonics, sub-ice topography, and the ice flow.

Tectonics

The pronounced west-east lineament (L1) represents an escarpment, as shown by the surface slope image and the DEM (Figs. 7 and 4), and provides the sub-ice obstruction responsible for the meteorite concentrations at the Elephant Moraine Icefield and the ice fields at the Reckling Peak Moraine. This escarpment seems to be part of a dissecting lineament, possibly extending from the Antarctic interior to the center of the Ross Sea area where it appears to join up with a lineament described in Coren et al. (1997). The pronounced south-north oriented escarpment to the west and northwest of the Allan Hills (L2) provides, in a similar fashion, the sub-ice obstructions (see Figs. 4 and 7) responsible for the meteorite concentrations of the AHI. L2 appears to have been displaced (sinistral motion) by L1. L1 and L2 appear to be of at least Jurassic age, since the magmatic body of Reckling Peak (Ferrar Dolerite of Jurassic age) had risen at their intersection.

The set of parallel ridge features west of the AHI are interpreted as evidence of block-faulted bedrock, presumably modified first (before the onset of Antarctic glaciation) by fluvial and later by glacial erosion, which is also the typical

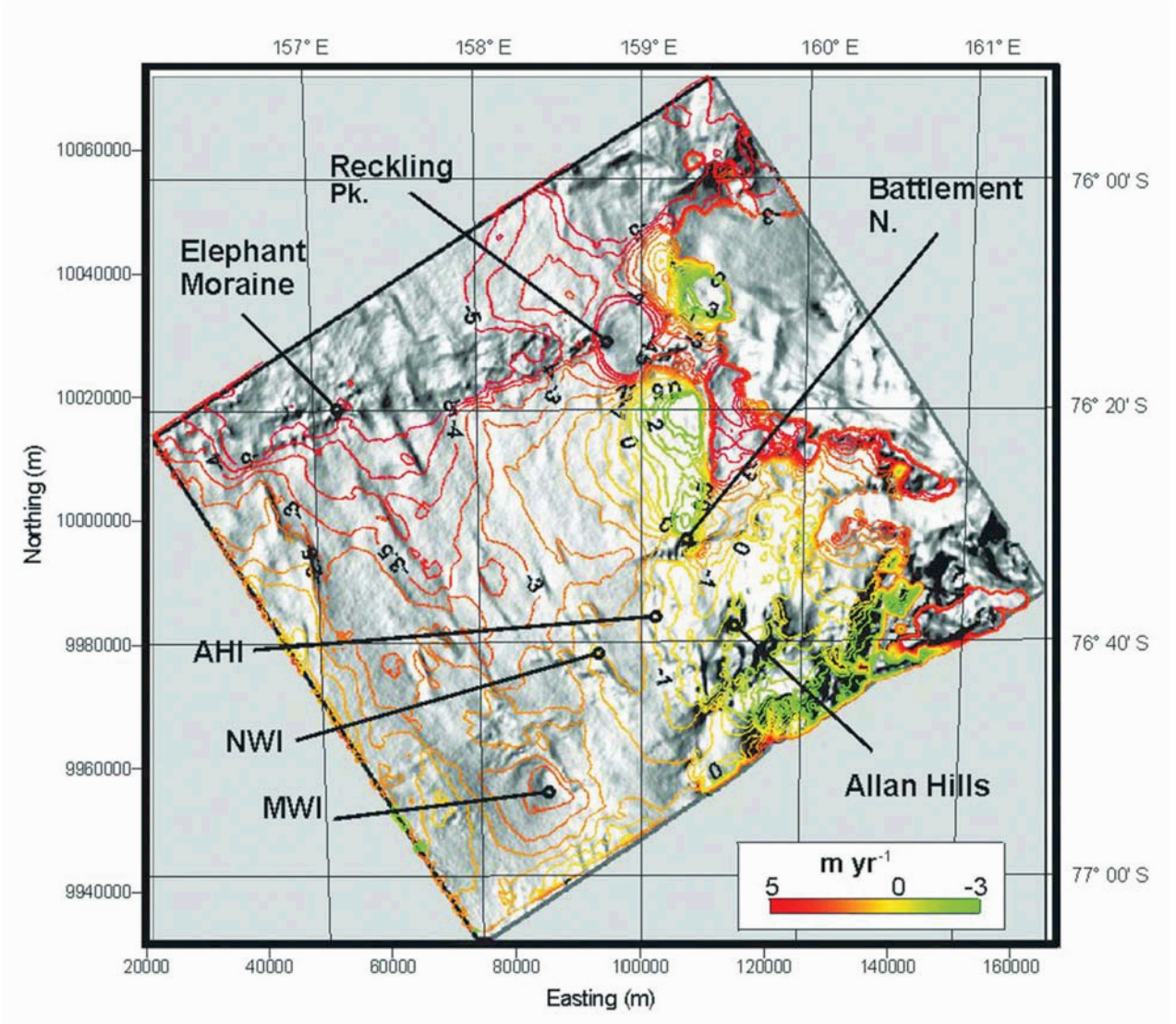

Fig. 6. Shaded relief representation of the digital elevation model with a superimposed ice flow velocity field contoured at a 0.5 m yr^{-1} interval. The SAR-derived velocity field does not contain information on direction of ice flow. Negative numbers on ice velocity contour lines denote ice flow predominantly to the north, positive numbers predominantly to the south.

tectonic style of the adjacent area to the north (Delisle 1997). The block-faulting suggested by the surface slope map is supported independently by an available radar profile between the MWI and NWI (Delisle and Sievers 1991), which shows extensive evidence for faulting of the bedrock (Fig. 8). The block-faulting is interpreted to have resulted from the uplift of the Transantarctic Mountains and the associated crustal extension during Cretaceous and Cenozoic times (Fitzgerald and Stump 1997). Erosional remnants of elevated ridges (presumably portions of block-faulted blocks) lie under the NWI and MWI and form the sub-ice obstructions necessary for the slowdown of ice flow and the build-up of meteorite concentration sites. The available radar survey of the AHI and NWI (Delisle and Sievers 1991; Delisle 1997) demonstrate the limited extent to which these former ridges have been modified by glacial erosion.

Ice Flow

A major bedrock rise exists below the AHI. Its shape, a mesa-type elevation incised at its rim by 4 valleys, is known from an extensive ground based radar survey (see Fig. 2 in Delisle [1997]). The only previously measured ice flow velocities in this area (see, e.g., Schultz et al. 1990) exist from repeat surveys of a triangulation network extending across the AHI (Fig. 9). In 1991, values of ~0.6 m yr^{-1} at the western corner of the blue ice of the AHI, of ~0.2–0.4 m yr^{-1} on the blue ice of the AHI, and of ~0.06 m yr^{-1} in the snow field

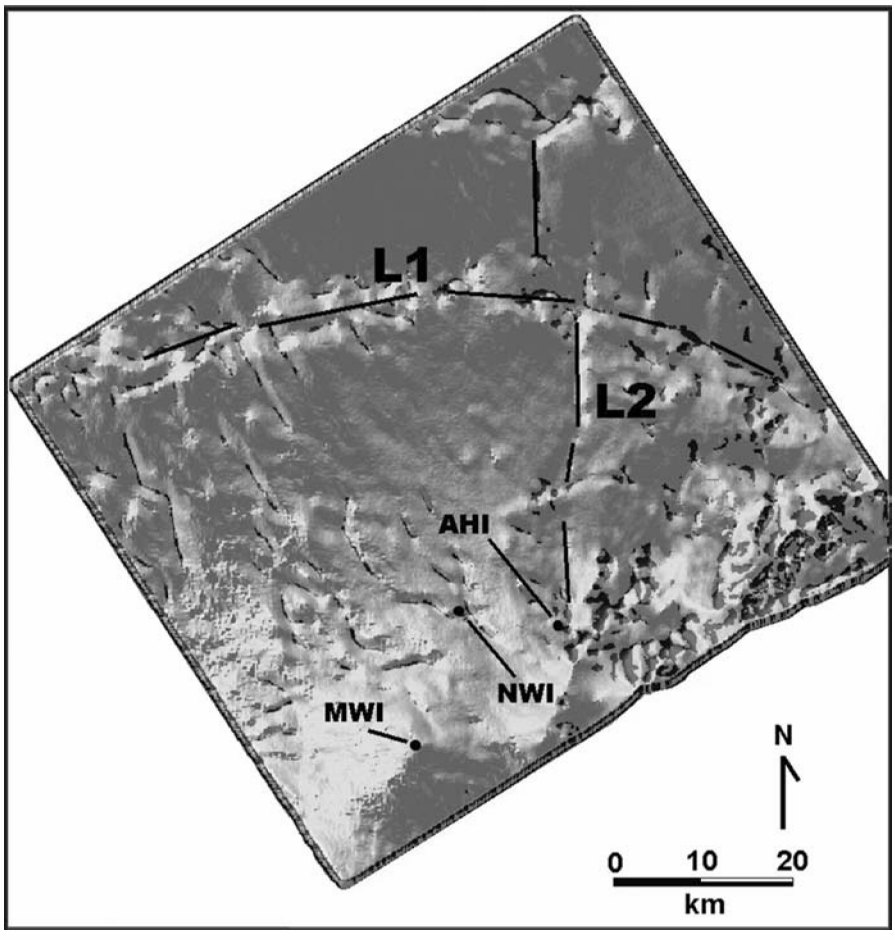

Fig. 7. Subset of the shaded relief representation of the DEM with marked major lineaments (L1 and L2). Note the sinistral displacement of L2 by L1. AHI: Allan Hills Icefield; NWI: Near-western Icefield; MWI: Mid-western Icefield.

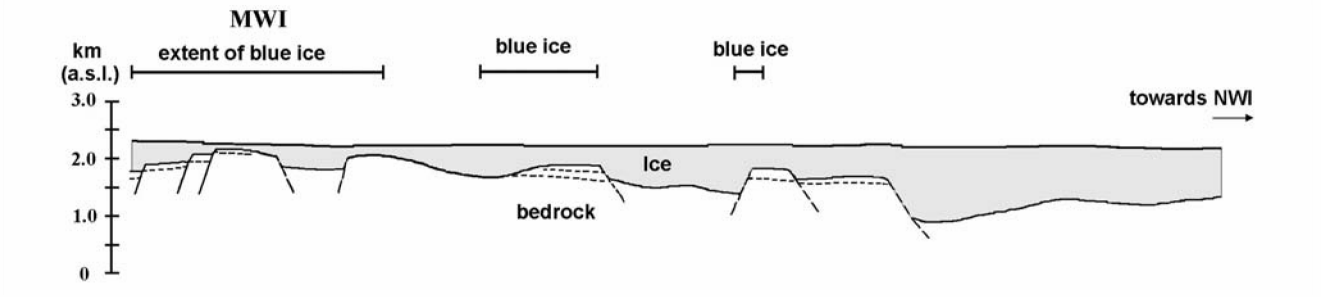

Fig. 8. Ground based radar profile from MWI toward NWI. Note the correlation between blue ice fields and bedrock rises (from Delisle and Sievers 1991).

depression along the western foot of the Allan Hills were reported. The SAR image, in general, confirms the slowly accelerating ice flow northward along the western foot of the Allan Hills, with velocities below 1 m yr^{-1}. The AHI is separated from the NWI to the west by an about 5 km wide ice stream (see Fig. 2 in Delisle [1997]).

The SAR image represents the NWI as an isolated ice rise, which is almost completely girded by the 1.5 m yr^{-1} contour line (Fig. 6). The course of the contour line can be interpreted as evidence of radial outflow of ice from the NWI. According to the memory of one of the authors (Delisle) of a field visit, the snow surfaces appeared to drop from the center of the NWI in all directions (but correctly assessing snow surface slopes is inherently difficult in snow terrain with no particular fixed points). A small blue ice depression (identical with the meteorite concentration site), which measures only

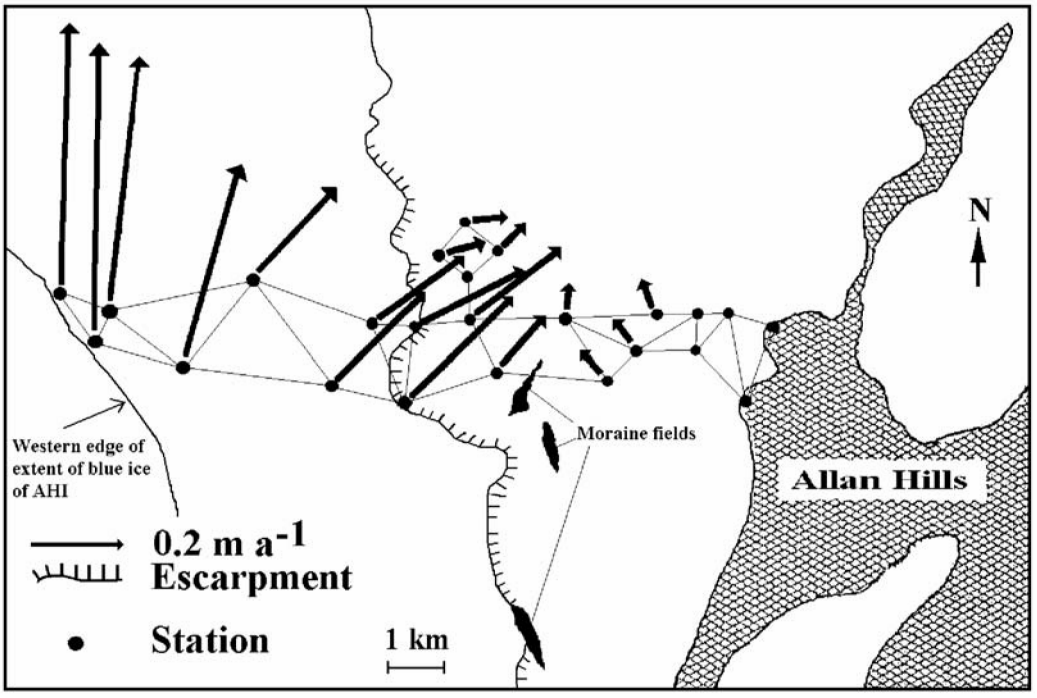

Fig. 9. Ice flow velocities to the west of the Allan Hills as measured by a triangulation survey (from Schultz et al. 1990).

an estimated 0.3 × 0.5 km area, exists to the northeast of the NWI and draws ice from all sides. The "radius of influence" of this depression is apparently too small for recognition by the SAR, since it has not picked up this local feature.

The distribution of ice flow lines in Fig. 6 also suggests outward ice flow from the center of MWI to all sides. The area in which the elevated velocities in comparison to the regional flow field are apparent measures roughly 500 km^2. We have no data concerning the FWI, but this very large blue ice field likely shows the same characteristics as the MWI.

The SAR-interferometry method identified, at the Elephant Moraine site, an east-west oriented escarpment and systematically accelerating ice flow toward this site. The high velocities (4–5 m yr^{-1}) south of the EM area most likely are due to the flow acceleration by the higher than regional ice slope angle across the escarpment. Most of the ice presumably crosses the EM area (unless sublimated) and moves onward to the north, with an ice velocity of ~5 m yr^{-1}, to the catchment area of the David Glacier. The predicted ice flow conditions at the EM site are in complete agreement with earlier descriptions of the regional ice flow conditions (Faure and Taylor 1985). Therefore, we consider the overall image of the ice flow velocity fields derived by the SAR method to be reliable, in particular, where systematic ice flow acceleration or reduction was mapped over large areas.

The EM site probably serves as the final effective obstacle to meteorite-rich ice and represents the last meteorite concentration site along the regional line of ice flow. Blue ice fields to the north near Ambalada Peak and Brimstone Peak are known for their lack of meteorite concentrations.

Estimates on the Regional Ice Thickness Distribution and Present and Past Ice Flow

The measured ice flow velocities in conjunction with the regional ice slope can be used to estimate roughly the average thickness of the ice in the region by applying the generalized ice flow equation (1) as formulated by Nye (1952):

$$u_s - u_b = 2A(T)\,(\rho g \sin \alpha)^n\, h^{n+1} / (n+1) \qquad (1)$$

u_s = ice velocity at the surface of the glacier (m s^{-1})
u_b = ice velocity at the base of the glacier (m s^{-1})
A(T) = temperature dependent flow law parameter of ice (s^{-1} kPa^{-3})
r = ice density (kg m^{-3})
g = gravitational acceleration (m s^{-2})
a = surface slope
h = ice thickness (m)
n = 3

Second, the approximate slowdown of ice flow in the region during the last cold stage can be deduced from this analysis. For the current situation, a mean annual ice temperature of –24°C at the ice surface (see, e.g., Jones et al. 1999) and a mean surface slope of 0.1° (the mean slope between MWI and the EM) or, alternatively, of 0.4° typical mean slope from

ice rises to the surrounding snow plains) are assumed. The values for the ice flow law parameter were calculated for ice temperatures estimated on the basis of an internal temperature gradient in the glacier of 28 K km^{-1} (equivalent to a basal heat flow density of 60 mW m^{-2}). The ice flow velocity (u_s) as function of ice thickness (h) (Table 3) was calculated assuming $u_b = 0$ (equivalent to a glacier frozen to the ground). This assumption is not valid in cases where ice thickness should be sufficient to facilitate wet-based basal conditions and basal gliding.

The analysis suggests ice thickness values slightly in excess of 700 m in areas where ice flow velocities of >2.5 m yr^{-1} occur. The SAR image suggests ice flow velocities of about 2.5 m yr^{-1} for the area between the MWI and NWI, for which a radar profile (Fig. 8) is available. The calculated ice flow velocity of 1.5 m yr^{-1} for 700 m thick ice is in reasonable agreement with the measured ice thickness values in the area away from bedrock rises with an ice surface slope of ~0.4°.

Equation 1 can also be used to estimate the ice velocities during cold stages, when ice temperatures about 7°C to 10°C lower than today existed (see, e.g., Jouzel et al. 1987). Table 4 shows the calculated u_s values for a mean annual ice temperature of −31°C. This evaluation suggests a reduction of ice flow velocities by a factor of ~3 in cold stages versus warm stages for the area. The likely reduction in ice surface slope during cold stages is not included in the values of Table 2. The advance of the Ross Ice shelf and the overall cooling of the ice shield in glacial times reduced the capability of outlet glaciers to discharge ice into the Ross Sea (see, i.e., Delisle 1993). The ice stand in the Transantarctic Mountains rose, in consequence, and surface slopes most likely were reduced by different degrees in different regions with the likely consequence of a further reduction of ice flow velocity.

INTERPRETATION

The scenario that emerges from the above consideration is one of an area with ice thickness values in excess of 700 m and ice flow velocities of 2.5–5 m yr^{-1}, stretching from the MWI to the EM. This ice moves preferentially northward and across the EM. This area is surrounded by a horseshoe-shaped area with low surface slopes and ice flow velocities of ≤2.5 m yr^{-1}. Elongated ridges rise to near the ice surface in both areas. They are the cause for the existence of blue ice areas and meteorite concentration sites wherever they are located in the areas of slow ice motion and, to a lesser extent, in the areas of fast ice flow (>2.5 m yr^{-1}).

The fact that these ridges express themselves as humps in the snow/ice surface is an indication of current thinning of the regional ice layer, which is caused by systematic ice drainage to the north. Ice from areas with thick ice can flow away faster (see Tables 1 and 2 for comparison) than ice from areas with thinner ice over bedrock rises. The impeded ice drainage from

Table 2. List of elevation data (sources in text) applied as ground control points for the construction of the DEM.

Latitude	Longitude	Elevation
–76.6330	159.7480	1945
–76.5895	159.1570	2015
–76.6555	159.2980	2040
–76.3105	159.1150	2020
–76.3480	157.6120	2022
–76.2655	157.5460	2022
–76.6270	158.2240	2072
–76.7185	159.5770	1950

Table 3. Theoretical ice flow velocities as a function of surface slope and ice thickness for ice during a warm stage.

h (ice thickness in m)	u_s (m yr^{-1}) for slope = 0.1°	u_s (m yr^{-1}) for slope = 0.4°
300	$1.6\ 10^{-4}$	$1.0\ 10^{-2}$
500	$2.7\ 10^{-3}$	$1.8\ 10^{-1}$
700	$2.3\ 10^{-2}$	1.5

Table 4. Theoretical ice flow velocities as function of surface slope and ice thickness for ice during a cold stage.

h (ice thickness in m)	u_s (m yr^{-1}) for slope = 0.1°	u_s (m yr^{-1}) for slope = 0.4°
300	$5.9\ 10^{-5}$	$3.1\ 10^{-3}$
500	$1.0\ 10^{-3}$	$6.6\ 10^{-2}$
700	$6.4\ 10^{-2}$	$5.6\ 10^{-1}$

local bedrock rises, as in the case of the MWI, results in a local ice rise and radial ice flow away from the bedrock rises. This process is obviously of a temporary nature and should have been inoperative in times with colder climates. We propose that the ice, which now drains in a radial fashion, is the remnant of a higher ice stand during the last cold stage, when it moved in a more uniform fashion across the MWI site (see also Cassidy 1983; Zolensky 1998). The existence of the NWI ice rise could be interpreted as an indication of a current lowering of the ice level from a higher ice stand acquired during the last cold stage.

Figure 10 shows a principal sketch of the ice flow conditions at the NWI and MWI as it is observed in the field today. The prevailing wind direction is from the southwest. The wind produces, via ice sublimation, blue ice fields on top and on the lee side (northeastern side) of ice rises. Small ice depressions develop with time on the lee side (the principal meteorite concentration sites). This situation is depicted in an exemplary fashion in Fig. 5, where the ice elevation, the backscattering coefficient σ0 of the radar signal, and the occurrence of blue ice fields are plotted. Blue ice fields occur where the surface slopes face toward the northeast. If the ice rises are, to a large extent, reduced or even eliminated by higher ice stands during glacial (cold) stages, then, logically, ice would move across the area in a “flip-flop-mode” during glacial-interglacial cycles: uniformly forward in one

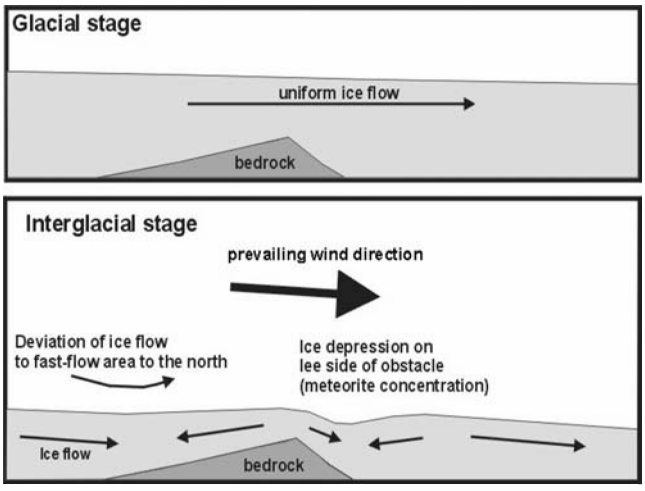

Fig. 10. Principal sketch of the changes in ice flow over bedrock rises during glacial and interglacial stages. Glacial stage: thicker ice moves uniformly over bedrock. (No particular meteorite concentration mechanism other than slow ice flow movement is operative.) Interglacial stage: thin ice covers bedrock rise, from which ice drains away in all directions and in particular to the north toward the fast ice flow area. Wind produces blue ice fields on the lee side of bedrock obstacle, which serve as the primary meteorite concentration sites.

preferential direction in glacial times and partially attracted back to the blue ice field depressions of the MWI and NWI (and FWI?) during warm stages. This theory is particularly attractive for explaining the high meteorite concentration on the AHI in comparison to MWI and FWI. Our ice flow velocity map indicates that the current source area of ice eventually moving onto the AHI is rather small in comparison to the other sites. Most ice seems to move past the AHI. From this point of view, the high meteorite concentration on the AHI with meteorites of very old terrestrial ages is, therefore, even more surprising (Nishiizumi et al. 1989; Scherer et al. 1997). The situation is different if some ice parcels, which have increased their internal meteorite concentration in one or several flip-flop modes on the MWI, NWI, and AHI (and FWI?), move not only past but also toward the AHI during cold stages. There, eventually, they are sublimated to a large extent because they are unable to escape again from the area due to the very low ice flow rates at the western foot of the Allan Hills in glacial and interglacial times alike.

Independent evidence exists for a higher ice stand in the region and, in particular, near the Allan Hills during glacial stages. Blue ice sloping away from the western foot of the Allan Hills today must have been transported to the site in the past. This blue ice is actively sublimated at this time and, therefore, was put in place during the last or one of the last glacial cycles. The higher ice stand in cold stages has apparently caused only minor spill-over into Manhaul Bay, the first valley to the east of the Allan Hills. Otherwise, the meteorite concentration on ice in Manhaul Bay would be higher.

CONCLUSIONS

The ~2500 km^2 region bounded in the south by the MWI, in the north by the EM area, and by the Allan Hills in the east represents an area of very moderate ice slopes. This area can be separated into 2 segments: a horseshoe-shaped area with ice flow velocities of ≤2.5 m yr^{-1} and a "faster" ice flow region, with ice flow velocities of between 2.5 m yr^{-1} and 5.0 m yr^{-1}, which is surrounded by the horseshoe area.

The tectonic evolution of this area resulted in a block-faulted platform with ridges, which were eroded down in the past and left remnants that serve as sub-ice obstructions today, which cause favorable ice flow conditions for the formation of blue ice fields and meteorite concentrations on the blue ice surfaces.

A simplified numerical model on ice flow and field observations alike suggests that the ice flow directions are likely to change in response to changes in the ice stand triggered by climatic changes. The ice flow conditions in the current warm (interglacial) stage appear to represent a deviation from the "normal" conditions that prevail during cold stages (which, in the past, represented much longer time periods than warm stages). Ice with a high meteorite concentration travels, possibly, in a flip-flop-mode across the area. In cold stages, ice flow is likely to be directed in a more uniform fashion to the north or northeast. In warm stages, some ice might be drawn back to regional blue ice fields on the lee side of ice rises.

Meteorites falling onto the horseshoe area have a chance to be moved with ice flow velocities of ≤2.5 m yr^{-1} in interglacial times in the vicinity of the FWI, MWI, NWI, or AHI. They are likely to be moved with an estimated velocity of ≤0.8 m yr^{-1} during cold stages, in a prevailing northward direction. Meteorites falling onto the "fast flow" area will either strand at the Elephant Moraine or move on to the catchment area of the David Glacier.

Editorial Handling—Dr. Scott Sandford

REFERENCES

Annexstad J. O. and Nishio F. 1980. Glaciological studies in Allan Hills, 1979/1980. *Antarctic Journal of the United States* 15:65–66.

Annexstad J. O. and Schultz L. 1982. Triangulation survey of the Allan Hills Icefield, 1981/1982. *Antarctic Journal of the United States* 17:57–58.

Bamber J. L. and Bindschadler A. 1997. An improved elevation dataset for climate and ice-sheet modelling: Validation with satellite imagery. *Annals of Glaciology* 25:439.

Benoit P. H., Sears H., and Sears D. W. G. 1993. The natural thermoluminescence of meteorites 5. Ordinary chondrites at the Allan Hills ice fields. *Journal of Geophysical Research* 98:1875–1888.

Cassidy W. A., Olsen E., and Yanai K. 1977. Antarctica: A deep-freeze storehouse for meteorites. *Science* 198:727–731.

Cassidy W. A. and Rancitelli L. A. 1982. Antarctic meteorites. *American Scientist* 70:156–164.

Cassidy W. A., Meunier T., Buchwald V., and Thompson C. 1983. Search for meteorites in the Allan Hills/Elephant Moraine area, 1982–1983. *Antarctic Journal of the United States* 18:81–82.

Cassidy W. A. 1983. The remarkably low surface density of meteorites at Allan Hills and implications in this for climate change. In *Antarctic earth science,* edited by James P. R. and Jago J. B. Canberra: Australian Academy of Science. pp. 623–625.

Cassidy W. A., Harvey R., Schutt J., Delisle G., and Yanai K. 1992. The meteorite collection sites of Antarctica. *Meteoritics* 27:490–525.

Coren F., Delisle G., and Rolf C. 1997. Evidence for Mesozoic-Early Cenozoic tectonic lineations in the Ross Sea and Transantarctic Mountains, Antarctica. In *The Antarctic region: Geological evolution and processes,* edited by Ricci C. A. Siena: Terra Antarctic. pp. 577–584.

Delisle G. and Sievers J. 1991. Sub-ice topography and meteorite finds near the Allan Hills and the Near Western Icefield, Victoria Land, Antarctica. *Journal of Geophysical Research* 96:15577–15587

Delisle G. 1993. Global change, Antarctic meteorite traps and the East Antarctic ice sheet. *Journal of Glaciology* 39:397–408.

Delisle G. 1997. Sub-Ice topography in selected areas of Victoria Land, Antarctica: Implications for its glacial erosion history. In *Geology and seismic stratigraphy of the Antarctic margin, Part 2,* edited by Barker P. and Cooper A. K. Washington D.C.: American Geophysical Union. pp. 127–135.

Faure G. and Taylor K. S. 1985. The geology and origin of the Elephant Moraine on the East Antarctic ice sheet. *Antarctic Journal of the United States* 20:11–12.

Fitzgerald P. G. and Stump E. 1997. Cretaceous and Cenozoic episodic denudation of the Transantarctic Mountains, Antarctica: New constraints from apatite fission track thermochronology in the Scott Glacier region. *Journal of Geophysical Research* 102: 7747–7765.

Fudali R. F. 1982. Gravity measurements across the Allan Hills main meteorite collection area. *Antarctic Journal of the United States* 17:58–60.

Gabriel A. K., Goldstein R. M., and Zebker H. A. 1989. Mapping small elevation changes over large areas: Differential radar interferometry. *Journal of Geophysical Research* 94:9183–9191.

Goldstein R. M., Engelhardt H., Kamb B., and Frolich R. M. 1993. Satellite radar interferometry for monitoring ice-sheet motion: Application to an Antarctic ice stream. *Science* 262:1525.

Harvey R. P., Dunbar N. W., McIntosh W. C., Esser R. P., Nishiizumi K., Taylor S., and Caffee M. W. 1998. Meteoritic event recorded in Antarctic ice. *Geology* 26:607–610.

Jones P. D., New M., Parker D. E., Martin S., and Rigor I. G. 1999. Surface air temperature and its changes over the past 150 years. *Reviews of Geophysics* 37:173–199.

Jouzel J., Lorius C., Petit J. R., Genthon C., Barkov N. I., Kotlyakov M., and Petrov V. M. 1987. Vostok ice core: A continuous isotope temperature record over the last climatic cycle (160,000 years). *Nature* 329:403–408.

König G. M., Winther J. G., and Isaksson E. 2001. Measuring snow and glacier ice properties from satellite. *Reviews of Geophysics* 39:1–27.

Kwok R. and Fahnestock M. A. 1996. Ice sheet motion and topography from radar interferometry. *IEEE Transactions on Geoscience and Remote Sensing* 34:25–37.

Nishio F. and Annexstad J. O. 1979. Studies on ice flow in the bare ice area near the Allan Hills in Victoria Land, Antarctica. *Memoirs of National Institute for Polar Research* 17:1–13.

Nishiizumi K., Elmore D., and Kubik P. W. 1989. Update on terrestrial ages of Antarctic meteorites. *Earth and Planetary Science Letters* 93:299–313.

Nye J. F. 1952. The mechanics of glacier flow. *Journal of Glaciology* 2:82–93.

Rignot E. J. M., Forster R. R., and Isacks B. L. 1996a. Interferometric radar observations of Glaciar San Rafael, Chile. *Journal of Glaciology* 42:279–291.

Rignot E. J. M., Forster R. R., and Isacks B. L. 1996b. Mapping of glacial motion and surface topography of Hielo Patagonico Norte, Chile, using satellite SAR L-band interferometry data. *Annals of Glaciology* 23:209–216.

Scharoo R. and Visser P. N. A. M. 1998. Precise orbit determination and gravity field improvement for the ERS satellites. *Journal of Geophysical Research* 103:8993–9001.

Scherer P., Schultz L., Neupert U., Knauer M., Neumann S., Leya I., Michel R., Mokos J., Lipschutz M. E., Metzler K., Suter M., and Kubik P. W. 1997. Allan Hills 88019: An Antarctic H-chondrite with a very long terrestrial age. *Meteoritics* 32:769–773.

Schultz L., Annexstad J. O., and Delisle G. 1990. Ice movement and mass balance at the Allan Hills Icefield. *Antarctic Journal of the United States* 25:90–94.

Van Heeswijk M. 1984. *Meteorite concentration by ice flow.* Columbus: Institute of Polar Studies. 68 p.

Whillans I. M. and Cassidy W. A. 1983. Catch a falling star: Meteorites and old ice. *Science* 222:55–57.

Zebker H. A., Werner C. L., Rosen P. A., and Hensley S. 1994. Accuracy of topographic maps derived from ERS-1 interferometry. *IEEE Transactions on Geoscience and Remote Sensing* 32:823–836.